CrystEngComm

Accepted Manuscript

ROYAL SOCIETY OF CHEMISTRY

www.rsc.org/crystengcomm

Cite this: DOI: 10.1039/c0xx00000x

www.rsc.org/xxxxxx

ARTICLE TYPE

Mesocrystalline Materials and the Involvement of Oriented Attachment – a Review

Lydia Bahrig, Stephen G. Hickey*, Alexander Eychmüller

Received (in XXX, XXX) Xth XXXXXXXXX 20XX, Accepted Xth XXXXXXXXX 20XX

DOI: 10.1039/b000000x

The latest advances in mesocrystal formation and non-classical crystallization of pre-synthesised nanoparticles have been reviewed with the focus on providing a fuller description of a number of complex systems and their properties and applications through examination of the crystallisation mechanisms at work. Two main crystallization principles have been identified; classical crystallization and particle based aggregation modes of non-classical pathways. To understand the non-classical pathways classical crystallization and its basics are introduced before non-classical pathways, such as oriented attachment and mesocrystal formation, are examined. In particular, the various destabilization mechanisms as applied to the pre-synthesized building blocks in order to form mesocrystaline materials as well as the interparticular influences providing the driving forces are analyzed and compared to the mechanisms at work within classical crystallization. Furthermore, the new properties of the mesocrystalline materials that derive from the collective properties of the nanoparticular building units, and their applications potential are presented. It is shown that this new class of materials has the potential to impact in a number of important areas such as sensor applications, energy conversion, photonic crystals as well as for energy storage, optoelectronics and heterogeneous catalysis or photocatalysis.

1. Introduction

Crystallization and crystalline materials play an important role in the areas of science and technology primarily because the inner structure of a material directly influences its properties. A well-known example is of course the different allotropes of carbon. In its diamond modification carbon is a transparent, hard material that does not possess electrical conductivity while in its graphite modification it is black, shows non-isotropic mechanical behaviour and is conductive within the plane of its covalent bonds.[1]

The differences in the properties of a material brought about by the different orientational arrangement of its component parts is extremely interesting and the controlled fabrication of one modification over another is clearly necessary for applications, as the device function and efficiency are usually based on the properties specific to a particular material modification. This is however but one reason as to why researchers are interested in gaining an understanding of the processes involved in classical crystallization. Already by the 18th century scientists had learned to use crystallization for purification and/or isolation of substances and thus as a means to gain access to compounds of high purity. Later the mechanism of single atoms, ions or molecules, which attach to crystalline surfaces during crystallization, was investigated. In comparison to the model of agglomeration, the processes that work during "real" crystallization are more complex, and up to now it has proven challenging for researchers to model accurately the theoretical pathways involved and to forecast the results of crystallization.

In the last decades additional interest has been paid to nanoparticulate materials and their arrangement in solids, as nanoparticles provide an additional class of "building block" that can be designed so as to possess new and tuneable properties caused by the quantum confinement of the electronic wave functions. In bio-mineralization, pathways which involve non-classical crystallization were discovered to exist and intermediates with highly oriented and symmetrically arranged building blocks in the nanometer region were established as being present, which later fuse to form iso-oriented or single crystalline materials. This has subsequently been further developed to encompass the principles of non-classical crystallization, which embraces new classes of materials such as iso-oriented materials or mesocrystals, which is the highly ordered arrangement of the individual building blocks into a three-dimensional superstructure. Additionally, these materials can be modified and their properties tuned and as such are of great interest for many applications.

To create, modify and optimize materials using methodologies involving non-classical crystallization first the dominant formation mechanisms need to be identified. One route of particular interest is to mimic the processes involved in bio-mineralization and superimpose upon their formation nanoparticular building blocks whilst maintaining the coincident arrangement of the building units. The routes that are presented in this review are based on first separately producing metal and semiconductor nanoparticles and

then their subsequent arrangement into highly ordered superstructures. We present the pathways of oriented attachment and mesocrystal formation focusing primarily on the advantages of their synthetic fabrication without however going into the details of the mimicry of bio-mineralization. We illuminate the various nanoparticular interactions and their role in providing the driving forces for arrangement and place them in context with respect to the different destabilization methods. First we begin by introducing the basic ideas behind classical crystallization and crystal formation principles and then discuss oriented attachment and mesocrystal formation. In a later section the analogy between classical and non-classical crystallization methods is highlighted and additionally the new properties, which are a combination of the properties of the individual nanomaterials and the new collective properties brought about by their assembly into quantum dot solids and their potential applications are presented.

2. Classical Crystal Growth

Before a description of some of the ideas connected with the process of non-classical crystallization, especially those of oriented attachment and mesocrystal formation, is embarked upon it is perhaps useful to reintroduce the reader to a number of the basic mechanisms involved in the description of classical crystallization. The main principle underlying classical crystallization is the ordered arrangement of material into a more stable crystalline structure (Ostwald rule of stages).[2,3] This may occur atom by atom, molecule by molecule or, in the case of salts, by the arrangement of ions *via* a precipitation reaction on an organic or inorganic nucleus and, in the case of unstable or metastable phases, *via* reprecipitation. The thermodynamic driving force for this process is solvent supersaturation, which is defined as the dimensionless ratio S (Equation [1]):

$$\boldsymbol{S = \frac{a}{K_{SP}}} \qquad [1]$$

where S is the relative supersaturation, *a* represents the concentration or more accurately the activity product of the individual components and K_{SP} represents the equilibrium solubility product.

2.1 Nucleation

As mentioned supersaturation plays a major role in the nucleation process. A number of different methods exist for the generation of supersaturated solutions such as influencing the solubility product by means of a temperature reduction or by changes in pressure. Another possibility is to influence the concentration or activity product by changing the pH value, adding a large amount of one of the components or by reducing the solubility of the component(s) through the addition of a non-solvent to the solution.[4,5] During this process nuclei will be created first before the particle growth begins. There are three different nucleation processes that lead to crystal growth: homogeneous nucleation, heterogeneous nucleation and secondary nucleation.[6] We will focus here solely on homogeneous nucleation, which is the simplest case. From a thermodynamic viewpoint, supersaturation, which is an energetically unstable state, is related to the change in chemical potential (Δμ) as outlined by equation [2] and therefore related to the overall free energy change involved:

$$\Delta\mu = -\boldsymbol{kT \ln S} \qquad [2]$$

where *k* is the Boltzmann constant, *T* the temperature and *S* the supersaturation. The change in the overall free energy during the nucleation process (Equation [3]) is the sum of the free energy due to the formation of new volume ($\boldsymbol{\Delta G_V}$) and the free energy which is required to create new surface ($\boldsymbol{\Delta G_S}$):

$$\boldsymbol{\Delta G = \Delta G_V + \Delta G_S = -\frac{4}{3}\pi r^3 \rho_S T \Delta\mu + 4\pi r^2 \sigma} \qquad [3]$$

In the above equation σ is the specific free interface, ρ_s is the density of the solid material and *r* is the radius of the nucleus. In Figure 1 the overall free energy during nucleation is shown and the profile of the function shows a positive maximum which corresponds to the critical radius r^* (Equation [4]).

$$\boldsymbol{r^* = \frac{2\sigma}{p_s|\Delta\mu|}} \qquad [4]$$

Nuclei sizes with $r > r^*$ will further grow and form stable entities as they can overcome the activation energy barrier at the critical radius. For a given supersaturation (*S),* the critical radius can be calculated and with a higher degree of supersaturation r^* becomes smaller, as can be shown by combining equation [4] with equation [2].

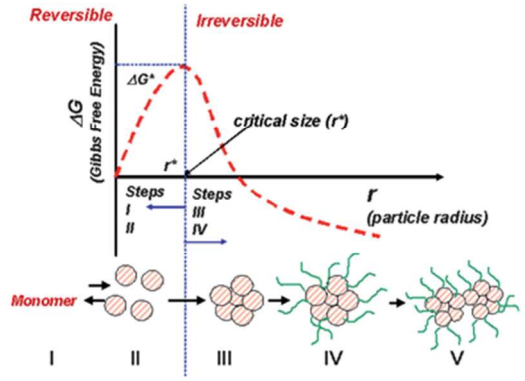

Fig. 1 Schematic diagram of the nucleation and growth process showing the five stages (from monomer to ligand-capped nanoparticles) and the dependence of the Gibbs free energy (G) on the crystal size. Below a critical radius (r*), a reversible process occurs; for r > r* the process becomes irreversible.[7]

When the concentration of the growth species decreases below the level where nucleation spontaneously takes place, the nucleation stops and only crystal growth will appear, as is the case described by the LaMer model in Figure 2.[8] If the time taken for the spontaneous nucleation is very short and further nucleation is inhibited, particle solutions with small size distributions can be produced, as is often the case in colloidal synthesis. High monodispersity can be achieved in this process through self-focusing of the colloidal size distribution. The smaller particles grow more quickly than the larger ones due to the higher free energy that acts as the driving force in the region of the critical size. Very monodisperse particle solutions can therefore be produced by quickly stopping the reaction.

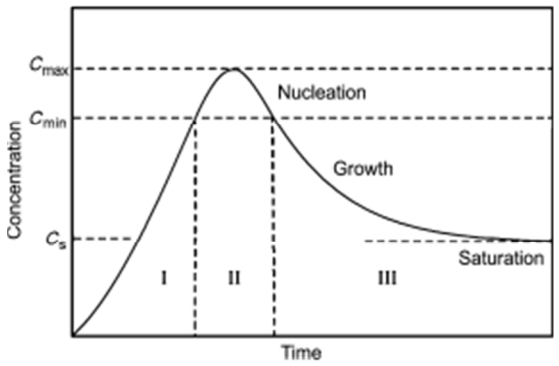

Fig. 2 LaMer and Dinegar's model used to describe nucleation and nucleus growth[9]

For reactions with longer growth periods Ostwald ripening can occur as, due to the decreasing supersaturation occurring in the reaction mixture, the critical radius of the particles is constantly moving towards larger sizes, with the result that stable particles move into the unstable regime and therefore again begin to dissolve. Hence, the larger particles will further grow at the expense of smaller ones which eventually leads to a broader, often bimodal, size distribution.

2.2 Crystal Growth

For the purposes of this work, the working definition of crystals or crystalline materials as being solids with regularly arranged atoms, molecules or ions will be used. It is of interest to note that the definition of a crystal previous to 1992 was that of a three-dimensional periodically arranged material with the smallest structural unit being the unit cell. While this definition adequately describes single crystalline materials, with the discovery of quasi crystals this definition was no longer deemed to be of sufficient precision. Therefore, in 1992, the International Union of Crystallography (IUCr) defined crystals with respect to their discrete diffraction order i.e. over their long range arrangements and which therefore allowed the inclusion of both polycrystalline materials and quasi crystals.

Single crystalline materials are seldom found in nature due to the inclusion of impurities and grain boundary defects. Even under relatively stringent laboratory conditions single crystalline materials are quite difficult to produce and often require a high technical outlay for their production.

The unit cell is the smallest repetition unit in a crystalline material and its structure the symmetry of which strongly influences the morphology of the crystal and is always a parallelepiped of precise size and defined angles. The resulting crystals very often possess the habit of polyhedrons with smooth surfaces and fixed angles which, due to the unit cell are constant for any one material. This is as a result of the correspondence principle of the morphological structure and the inner arrangement of crystalline material, where the lattice planes of the crystal are parallel to the crystal surface. The morphology of the resultant crystal can be predicted using Wulff's model, which was established at the beginning of the last century.[10]

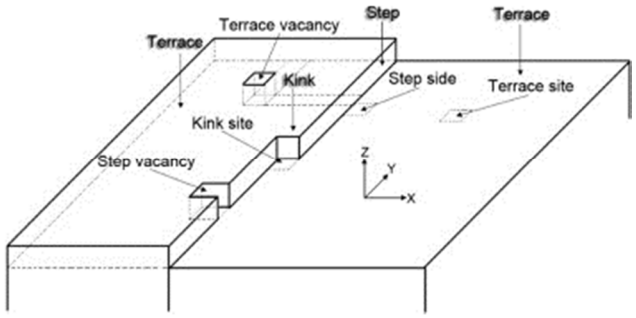

Fig. 3 Schematic diagram of the substrate surface described by the Kossel–Stranski "terrace-step-kink" model.[11]

Which crystal surface finally dominates depends on the relative rates of growth of the different crystal facets. The more slowly growing facets will be present at the end of the growth period, as the faster growing crystal facets, which have a high surface energy, will have been eliminated. In addition, during crystallization the physical and chemical environment is important for the resulting habit of the crystal. Different additives or physical parameters influence the rate of growth of the single crystal facets and indirectly influence the morphology, a process known as exomorphism. At the end of the crystallization process, the single crystal facets have the same vapour pressure and the resulting structure, which is then termed the equilibrium form, is the form that shows the lowest surface energy in comparison to equivalent crystals of the same volume. During the growth process atoms, molecules or ions are arranged on the surface of the crystal structure and hence the building blocks can attach to a number different positions on the crystal face. As is described in the Kossel–Stranski model (see Fig. 3) the building blocks arrange at a kink or on a step as these are energetically preferred[12] and as a result, the crystal facet will be assembled layer-by-layer resulting in the appearance of flat crystal surfaces at the end of the process.

3. Non-classical Pathways

3.1 Main Principles

The concepts and ideas behind non-classical crystallization are an attempt to describe an alternative notion of the formation of crystalline materials, according to which the crystallization does not undergo the classical pathway of nucleation and crystal growth *via* atom, molecule or ion deposition, but follows a particle mediated aggregation or self-assembly process.[13]

Both pathways start with particle formation induced *via* supersaturation which results in the formation of the initial building blocks and hence the variety of building blocks that may be present is quite large. Not only may crystalline building blocks be used for non-classical crystallization, but so too can amorphous[14–19] and liquid structures[20–25]. In the case of crystalline building blocks, the classical growth mechanism is inhibited due to the reaction species reaching their equilibrium solubility[26] or because of the temporary stabilization of the nanoparticles. Different steps within the non-classical crystallization pathway have been identified and, as we are still in the initial stages of our understanding of the processes involved in non-classical crystallization, it is quite likely that the list is not as yet complete. The steps identified thus far include:

- the formation of primary building blocks such as intermediary clusters or, as in the case of liquid precursors, phase separation
- the mesoscopic transformation of superstructures, which have formed from amorphous building blocks
- the oriented attachment of nanoparticles
- the formation of three dimensional mesocrystals *via* the self-organization of organic-inorganic nanoparticles

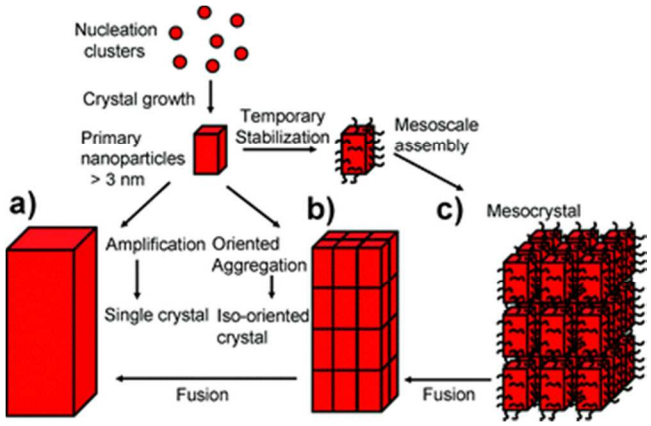

Fig.4 Schematic representation of both classical and non-classical crystallization. (a) Classical crystallization pathway, (b) oriented attachment of primary nanoparticles forming an iso-oriented crystal upon fusion, (c) mesocrystal formation via self-assembly of primary nanoparticles covered with organics.[27]

These four steps[13] are illustrated in Fig.4 with the classical crystal growth process presented by path (a) where primary nanoparticles when synthesized *via* atom, molecule or ion precipitation grow to afford large single crystals. Path (b) describes the mechanism of oriented attachment where, following post-structuring on the mesoscale, it is possible with mesoscopic transformation to generate single crystals from iso-oriented crystals. For path (c) to occur it is necessary for temporary stabilized building blocks to be present. These inorganic cores with their accompanying organic ligand or stabilizer shell can be structured on the mesoscale in three dimensions. After initial fusion, it is possible to generate iso-oriented crystals and finally single crystals. The production of mesocrystals *via* non-classical crystallization from a variety of different materials such as PbS[28–30], CdS[31], CdSe[32,33], Au[34], Ag[35], $BaCO_3$[36,37], $CaCO_3$[15,38–46], $CoC_2O_4 \cdot 2H_2O$[47], $CoPt_3$[48], and D,L-alanine[14,49] has been observed and shows a high degree of ordering containing well aligned nanoparticular units. Additionally, these materials have been observed to possess scattering properties that are similar to single crystals.

Non-classical crystallization occurs predominantly in biological systems or during biomineralization where nucleation and growth of the amorphous precursor phase (building blocks) and their subsequent aggregation into highly ordered and aligned structures can simultaneously take place.[50,51] An example of this is the sea urchin spine, where amorphous precursors crystallize to form nanoparticles whose sizes are limited by impurities that inhibit infinite crystal growth. The impurities surround the nanoparticles and act as new nucleation centres for the formation of additional and arranged nanoparticles, which leads to mesocrystal formation with interlinking bridges.[27] Hence, hybrid materials with specific and distinct properties can be generated under ambient conditions.

The definition of synthetically prepared mesocrystals includes that not only do the materials contain a high degree of ordering of the inorganic-organic hybrid material building blocks but additionally, the nanoparticles (building blocks) should possess a mutual alignment along a common crystallographic axis.

In such cases, mesocrystals form a specific class of quantum dot solids in which there is a growing appeal as the interesting properties derived from combining tailored nanoparticular characteristics with properties which derive from the nanoparticle arrangement may provide made-to-measure material solutions in a number of important application fields. Tuneable properties such as photonic band gaps, electronic and optical properties, and high surface area make these materials interesting for applications as diverse as biomedicine, solar energy or energy storage, optoelectronics and heterogeneous catalysis or photocatalysis.[52]

3.2 Oriented Attachment

Bottom-up approaches for nanoparticle synthesis are nowadays quite common and have gained in importance for both materials science research and applications. Therefore the control of the morphology, particle size and size distribution of the prepared colloidal solutions is of great consequence and, as these processes are well described by the classical nucleation and crystal growth theory, theoretical modelling of the crystal growth is possible. With increasing reaction time, the size distribution of the colloidal solution becomes broadened in a process known as Ostwald ripening.

Penn and Banfield have determined that not all growth processes present in nanoparticular solutions can be described using this model.[53–55] For example, TiO_2 particles in hydrothermal synthesis grow together along a crystallographic fashion and form one-dimensional arrangements, the as-synthesized nanoparticles working in this case as building blocks. The driving force for this agglomeration, which is nowadays called oriented attachment, is the reduction in the surface energy achieved by fusion of the facets which possess the highest surface energy. For this process two main principles are postulated (i) fusion can take place after the effective collision of oriented nanoparticles or (ii) coalescence can be induced by particle rotation.[56]

For the first mechanism to occur, the colloidal solutions must be well dispersed in order for oriented attachment to be able to take place and high collision rates and free rotation of the nanoparticles must occur. Colloidal solutions are normally kinetically stable with repulsive forces between the particles hindering agglomeration. Under these conditions, the oriented attachment growth rate is related to the number of effective collisions and to the minimization in the number of high-energy facets *via* the reduction of the surface energy.[57,58] An effective collision is defined as a collision that results in an irreversible oriented attachment. Therefore, the different orientations of the nanoparticles during

collision need to be aligned, in order for fusion to a congruent two-dimensional structure at these interfaces to be possible.[59–61] Collisions, where the orientation is not suitable for coalescence or which do not lead to irreversible attachments are termed non-effective collisions.

Superstructures of different dimensionalities can be synthesized through oriented attachment based on nanometer sized building units, which can be treated as zero-dimensional entities, such as spheres, polyhedrons and cubic structures. Thereby, one-dimensional wire or rod like structures, two-dimensional plates and also three-dimensional self-assemblies can be formed *via* arrangement of the nanosized building blocks.[62,63] One-dimensional structures are primarily generated through oriented attachment based on collisions. Hence, interparticle interactions are possible between 0D and 0D particles as are, in the case of the formation of 1D structures, also interactions between 0D and 1D structures and 1D and 1D structures.[13,64] These collision processes are statistical and as a consequence superstructures with different growth directions can be observed.

The second pathway for oriented attachment to occur is not controlled *via* collisions, but rather dominated by particle interactions in the short- and medium-range. In this range, the attractive forces such as van der Waals forces are greater than the repulsive forces such as electrostatic interactions or steric hindering. Normally these interaction conditions are observed in weakly flocculated colloidal states. The rotational freedom of the single nanoparticles is important to bring about the alignment of the nanoparticles along a crystallographic fashion.

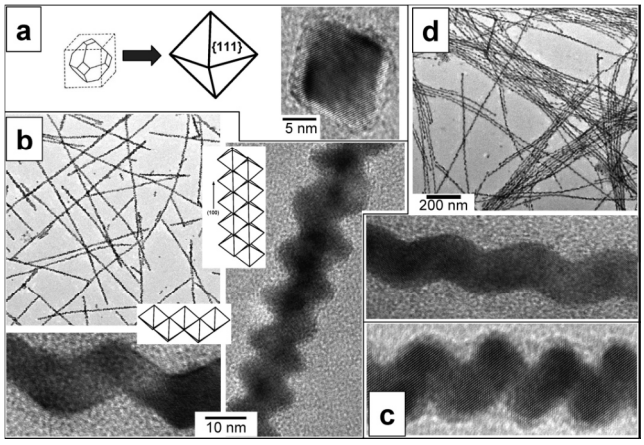

Fig. 5 (a) Octahedral PbSe nanocrystals grown in the presence of HDA and oleic acid. (b) TEM and high-resolution TEM images of PbSe zigzag nanowires grown in the presence of HDA. The cartoons show packing of octahedral building blocks to form the nanowires. (c) HRTEM image of single- crystal helical PbSe nanowire grown in oleic acid/HDA/trioctylamine mixture. (d) Helical nanowires formed upon annealing of straight PbSe nanowires, as shown in Figure 1c, in the presence of trioctylamine.[65]

The first step of this reaction path is the interaction of 0D and 0D primary structures to form 1D and 2D architectures. After this formation step, a second phase occurs *via* the formation of 2D (from 1D structures) or 3D structures *via* self-assembly of the 1D and 2D architectures. This hierarchical process can produce mesocrystals in an intermediate state before mesoscopic transformation take place and iso-oriented crystals are formed.[66]

The growth processes described above and the resulting morphologies of the superstructures can be additionally influenced by the presence of organic additives. As is postulated in Wulff's facet theorem[67], (i.e. at equilibrium the crystal structure with the lowest surface energy by constant volume develops and as a result, the crystal structure reflects the intrinsic symmetry of the lattice) most metals show cubic crystal growth instead of rod like structures.[68,69] As described above the growth rate of the different facets can be altered by influencing the surface energy i.e. by adding organic molecules, through which the crystal morphology can be indirectly influenced. Another possibility by which the morphology can be influenced is by using organic molecules as templates for 2 or 3-dimensional superstructures.

Cho *et al.*[65] reported on nearly defect free PbSe nanowires through assisted assembly using organic molecules. With different combinations of additives straight, helical, branched, tapered and zigzag nanowires can be formed, (shown in Fig. 5) as can nanorings. Not only was the oriented attachment influenced by these organic molecules but the nanoparticle synthesis was also modified through the addition of long-chained, aliphatic primary amines such as hexadecylamine, dodecylamine and oleylamine and finally octahedrally shaped nanoparticles were synthesized that contained solely {111} facets, see Fig. 5a.

Using another method Kotov *et al.*[70] have nicely shown the stepwise progress of the oriented attachment of CdTe nanoparticles to highly luminescent crystalline nanowires. Washing steps induce destabilization of the CdTe nanoparticles by first removal of the stabilizing ligand molecules and subsequent one-dimensional agglomeration. A strong dipole-dipole interaction is believed to be the main driving force for the self-assembly. After arrangement into 1D structures a recrystallization process from the cubic zinc blende structure to the more stable hexagonal wurtzite structure takes place. This phase transition does not greatly influence the luminescence properties of the as-synthesized nanowires with only a small red shift occurring due to a loss in confinement in the growth direction of the wires.

Pacholski *et al.*[71] have reported on single crystalline ZnO nanorods prepared *via* oriented attachment using quasi-spherical ZnO nanoparticles as building blocks. The arrangement takes place along the c-axis and primarily bottle-neck structures have been presented. Under the reaction conditions (reflux) communicated, additional conventional growth mechanisms such as dissolution and growth of the monomers act to smoothen the rod surface so that highly parallel crystal facets result.

Not only is oriented attachment possible for semiconductor nanoparticles but it can also be employed in the case of metallic nanoparticle systems. For example, Ravishankar *et al.*[72] have reported on the formation of ultrafine single-crystalline gold nanowires by the controlled removal of primary capping ligands (oleylamine) from the {111} facets using ascorbic acid which leads to the destabilization and resulting aggregation of the gold nanoparticles in one dimension. This method works especially well

for gold nanoparticles as the gold-amine binding energy varies for the different facets. The resulting anisotropic structures show convex-concave surfaces with differences in their chemical potential and which leads to a smoothing of the surface along the wire.

The above-mentioned examples highlight only a small selection of the possibilities of employing oriented attachment. In addition to oriented attachment processes involving organic additives, oriented attachment without the help of so called assemblers is also possible. The oriented attachment mechanism is one of the more important non-classical crystallization pathways as it provides the ability to produce crystal architectures which cannot be produced *via* classical crystallization methods, opening a wide field of potential applications. Presently, we are far from comprehensively understand the growth processes and therefore lack the ability to systematically influence them. That is indeed why additional experimental and theoretical research is essential i.e. to shine more light onto these processes in order to enable further design of new materials using this fascinating growth mechanism.

3.3 Mesocrystal Formation

A second means of non-classical crystallization is the formation of mesocrystals. Mesocrystals are crystalline materials with crystal facets of some hundred nanometres up to the micrometre size regime. The smallest building units are normally colloidal, crystalline nanoparticles with a core-shell structure, composed of an inorganic core with an organic stabilizing shell. These building blocks are arranged in a unit cell, which forms the entire mesocrystal *via* a translational shift and which results in an inner crystalline structure analogous to that of single crystals. With these nanoparticular superstructures single crystals can be formed during a fusion process *via* the formation of an iso-oriented crystal to produce single crystals as shown in Fig.4.[73]

With this distinctive architecture new material properties can be derived because, as mentioned previously, the nanoscopic effects are still present within the individual building blocks of the macroscopic mesocrystal as are new properties which derive from the collective interactions of the building units. It is this combination of properties that is of great interest for many applications, amongst which are those based on photonic band gaps[74] or tuned electronic and optical properties in the case of semiconductor building blocks[75].

Aggregates of particles have been observed since the first crystallization experiments, but normally they were not observed to display any homogeneous architecture or size and the main focus of the research in this period of time lay in investigating various aspects of the classical pathway. In the last few decades however, partly due to the improved analysis methods, these particle agglomeration processes have been more intensively examined. Amongst the first experiments on mesocrystals without defined habit were undertaken by Matijevic *et al.* and were concerned with various Ce(IV)-salts in a crystallization study in the absence of organic additives[76], where it was observed that the elongated, and also plate-like nanoparticles, orient themselves along one axis to form a one-dimensional superstructure. Earlier, Petres *et al.*[77]investigated geometrically shaped mesocrystalline $BaSO_4$ architectures containing a porous inner structure, which would normally be expected to exhibit growth according to classical crystallization principles similar to that of a single crystalline material. Studies on different materials such as CuO[78,79], CeO_2[76], MgO[80,81], Fe_3O_4[82] and Eu_3O_4[83,84] show the variety of possible structures. In addition to the aforementioned materials, $CaCO_3$ was also observed to form mesocrystalline materials. This $CaCO_3$ structure, which was synthesized in silica gel and known as the "sheaf-of-wheat", was described by Dominquez *et al.*[85] in which calcite rhombohedra orient along the c-axis. The complete structure behaves as a single crystal under a polarization microscope, which can be used to visualize the perfect arrangement of the rhombohedra building units.

Nevertheless, not only are one-dimensional arrangements and two-dimensional nanoparticular arrays[86–92] possible, but so too are three-dimensional mesocrystals. Busch and Kniep demonstrated a nearly perfectly arranged 3D fluorapatite mesocrystal, synthesized in gelatin.[93–98] The resulting elongated hexagonal mesocrystals showed typical single crystalline properties, which makes it difficult to determine the arrangement of the building blocks. Only with perpendicular thin cuts could the mesocrystalline structure be proven. The growth mechanism of these fluorapatite crystals was not influenced by the 2 w% of intracrystal gelatin, which was found between the building blocks.

The particular growth mechanism for these kinds of arrangements has not presently been fully elucidated. However, the growth of mesocrystals in gels seems to be appropriate , as in gels the local supersaturation is very high[99], which leads to the formation of the primary building blocks. The high viscosity present in these media slows down mass transport processes such as convection and other processes that influence crystallization and thus promotes the undisturbed orientation of the building blocks along their preferred interaction direction to obtain an energy-minimized structure.

Formation methods

Beside the synthesis of mesocrystals in gels,[46,98] there are a variety of alternative methods to bring about the ordering of organic ligand shell containing spherical nanoparticles, especially with respect to metal and semiconductor building blocks. The obvious starting point for these methods is the correct synthetic protocol to provide the required nanoparticles in sufficient quantity and monodispersity and in a solvent environment which can subsequently be used to bring about their controlled arrangement on the mesoscale.

Murray *et al.* have shown that with their layering technique the gentle destabilization of nanoparticle solutions by a slow diffusion of non-solvent into the solution leads to 3D crystalline structures.[4,75] During destabilization, the solution is kept in the dark and left until precipitation is complete thus ensuring that intermixing of the phases and convection effects are minimized, a process which is analogous to the use of gels as solvent. The solvent/non-solvent pair, the polarity of the non-solvent and the temperature are amongst the more important factors that influence the destabilization rate. Nagel *et al.*[100] have used the arrangement mechanism of Murray *et al.* and applied it to monodisperse lead

sulphide nanoparticles. An additional modification to the technique employed by Talapin *et al.* introduces a buffer-layer, which is normally a weaker acting non-solvent than the non-solvent layer above, between the solvent and non-solvent.[33] The buffer-layer acts to slow down the destabilization rate, due to the fact that the time taken for the first agglomeration of nanoparticles to occur is protracted, which results in better quality mesocrystals with respect to their size and their higher symmetry. In a step taken towards the optimization of the gentle destabilization method a recent additional study, in which it was shown that a capillary microfluidic platform, where the destabilization *via* non-solvent forms nanoliter microfluidic plugs, can be used for the self-assembly of inorganic nanoparticles into 3D superstructures and where additionally the growth kinetics could be studied, should be mentioned.[101]

It is not always necessary to destabilize the nanoparticles using a non-solvent in order to arrange them into ordered crystalline materials. Zheng *et al.* have used the inherently low stability of the nanoparticles in their reaction solution after the synthesis.[102] In this study the nanoparticles were kept in the reaction flask without the application of the clean-up procedure and the low solubility at reduced temperature lead to agglomeration and growth of the first nanoparticle arrangements over two days. A further method based on supersaturation methods is the slow and controlled evaporation of the solvent. Normally this method is quiet common for the preparation of 2D structures[27,90,103–108], but a number of examples exist where it has been employed to form 3D architectures [109–111].

To create oriented and ordered architectures, electrostatic interactions can also be used as has been shown by Grzybowski *et al.*[112–116] In these studies oppositely charged nanoparticles were slowly destabilized *via* solvent evaporation. At first an equal amount of oppositely charged nanoparticles is established by titration of the nanoparticles of interest. Then a number of cleaning procedures follow and the precipitate is dissolved in a mixture of solvent and non-solvent. During the slow evaporation of the lower boiling solvent, destabilization of the nanoparticles is initiated and the structural arrangement is driven by the oppositely charged ligand shell of the nanoparticles. In this destabilization method nanoparticles made of different materials can be arranged into macroscopic mesocrystals or, as they have been called in this case, supracrystals. This method has so far only been reported in aqueous solution as it is based on charge pairing and is therefore limited to polar solvents as otherwise the surface charge on the ligands will be lost.

Interparticle interactions

The methods thus far mentioned are based on the slow destabilization of nanoparticles in order to provide sufficient time for the building blocks to arrange. If the agglomeration occurs too quickly the resulting structures are usually not highly ordered but often non-ordered or porous. The particle arrangement during slow precipitation primarily takes place through interparticle interactions. As reported by Cölfen *et al.*, there are different possible mechanisms for mesocrystal formation. First, processes may be classified as to whether they are dynamic or static, with the above mentioned methods all falling under the heading of dynamic processes. During a static process, an organic matrix determines the outer shape of the mesocrystal formed and the building blocks assemble along the structures present. In dynamic pathways, which are more prevalent, the building blocks assemble freely into three-dimensional mesocrystals and, as is shown in Fig. 6, three different main pathways can be used to describe their formation.

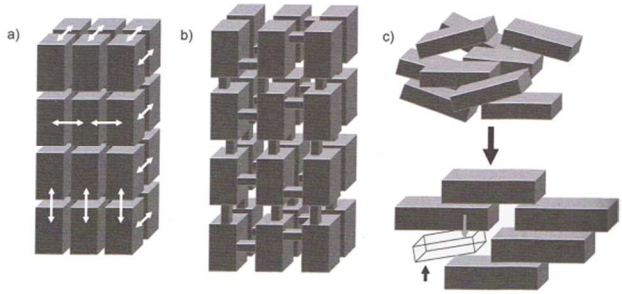

Fig. 6 Three principal possibilities to explain the three-dimensional mutual alignment of nanoparticles into mesocrystal: (a) nanoparticle alignment by physical fields or mutual alignment of identical crystal faces; (b) epitaxial growth of nanoparticle employing a mineral bridge connecting the two nanoparticles; and (c) nanoparticle alignment by spatial constrains, i.e. an entropy-driven mechanism.[13]

The first route is based on vectored physical interactions such as electrostatics and investigated by Grzybowski *et al.*[117] Other forces such as van der Waals interactions, magnetic interactions, entropic effects, attractive depletion forces, dipole interactions and a host of others can also influence the resulting structures during the agglomeration of the building blocks. The second mechanism is based on the three-dimensional arrangement through the formation of interparticle mineral bridges. These bridges occur after the classical crystallization of the nanoparticles has stopped thereby allowing the temporary stabilization in the form of ligand molecules to take place. Mineral bridges can then grow on defects in the ligand shell. A new nanoparticle can grow on the newly induced surface, up to the point of complete stabilization and resulting equilibrium. The growth mechanism between nanoparticle formation and defect induced mineral bridge growth varies.[50,118–120] The third pathway only occurs in the case of anisotropic building blocks and is based on the Onsager-theory of lyotropic liquids, where entropic forces result in ordered arrangements.

To understand the arrangement of nanoparticles with respect to the above mentioned preparation techniques, it is necessary to focus on the physical interparticle interactions as it is these that are important for the first pathway. Therefore, the different length scales and magnitudes of the interparticle forces will now be the main focus of our discussions before further examining the specific types of interparticle interactions.

The Lennard-Jones potential function is the predominant model used in predicting the interactions between atoms and small molecules, where the attractive interactions such as van der Waals act to counter the repulsive interactions which are mostly electrostatic in nature. The length scales of the attractive and

repulsive forces are of the same magnitude as the atomic, molecular or ionic building units to be used in the assembly. If we consider nanoparticular building blocks, this condition is no longer valid as while the length scales over which the interactions are effective remains constant the size of the building blocks has drastically increased. In principle, it would be possible to calculate the potential over all constituent atoms of the nanoparticle and their interactions with other nanoparticles, but this would be costly and likely to contain many errors because of the necessary oversimplification of the interactions or in the estimation of their numerical values.[117]

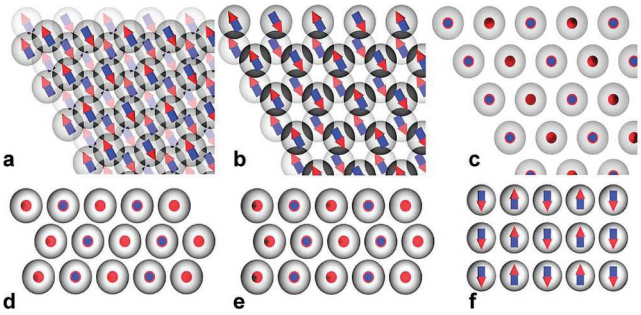

Fig. 7 Dipole ordering in nanoparticle superlattices. Top view ([0001] plane) of (a) horizontal antiferroelectric ordering in fcc, (b) horizontal antiferroelectric ordering in hcp, and (c) vertical antiferroelectric ordering in sh lattices. Panels (d), (e), and (f) show side views ([1h2 h] plane) of fcc, hcp, and sh structures, correspondingly.[107]

The varying ratio of the length scales of the interactions with respect to the particle sizes plays an important role during self-assembly. To influence self-assembly, the attractive forces need to be strong enough to overcome the entropic effects such as the loss of translational and rotational movement of the building blocks. Initially, the attractive interactions induce cluster formation and the early stage of this aggregation can be described within the equilibrium theory of physical clusters,[121] where the average numbers of n-sized clusters can be estimated. Additional agglomeration then follows, so that mesocrystals are formed. The agglomeration is an interplay between the length scale and the magnitude of all of the interactions involved. On the one hand short range interactions of high magnitude induce self-assembly whilst on the other long range interactions of small magnitude result in ordered arrangements. Exceeding a value of magnitude and interaction length within this ideal range results in the particle agglomeration occurring too quickly and consequently only non-ordered structures or those with short range order precipitate.[117] This interplay of the length scale and the magnitude leads to the different destabilization methods as have been presented above and the different interaction potentials lead to different equilibrium morphologies and structures of the resulting colloidal mesocrystals. We now focus on the most commonly observed interaction occurring between matter, namely the van der Waals (vdW) interactions. These non-covalent interactions are based on the electromagnetic variation within molecules or bulk materials. Normally, the vdW interactions are attractive and their magnitude can range from being quite small up to hundreds of kT, with the magnitude of their interaction decreasing as a function of the sixth power of their separation. Generally three different types of vdW interactions are distinguished:

- Keesom interactions (dipole - dipole interactions)
- Debye interactions (dipole – induced dipole interactions)
- London dispersion interactions (induced dipole - induced dipole interactions)

The vdW interactions are always present between materials and molecules and can lead to unintentional agglomeration between nanoparticles, which is why normally charges or ligands, which are employed to sterically stabilize the nanoparticular building blocks, are required. By contrast, this phenomenon can also be used for the controlled assembly of the nanoparticular units, as described in the works of Murray *et al.*[75] where fcc packed 50 µm large superlattices composed of 2 nm sized CdSe nanoparticles are formed mainly by vdW interactions. The non-uniformity of the vdW interactions can influence the directional arrangement caused by the different ligand coverage of the crystal facets of the single nanoparticles. Talapin *et al.*[107] have demonstrated that the dipole-dipole interactions influence the ordering of the nanoparticles and it was revealed that while antiferroelectric arrangements of dipoles is unusual for bulk materials, this type of arrangement can be found in the case of nanoparticular superlattices as is shown in Fig. 7. Goubet *et al.*[122] have also investigated Au nanoparticles that arrange with the help of vdW interactions during solvent evaporation and have found that these are not the sole interactions that influence the agglomeration process. Besides the vdW forces electrostatic forces and ligand-solvent interactions also control the assembly and resulting morphology.

In addition to the vdW interactions, the sum of which is normally attractive, electrostatic interactions, which provide attractive forces between oppositely charged building units and repulsive between like-charged nanoparticles, are also present. The intensity of these interactions during the self-assembly can be influenced by the concentration of nanoparticles in the solution, their charge and also by the dielectric constant of the solvent. Grzybowsi *et al.*[112–116] have investigated this in a number of self-assembly experiments involving gold and silver nanoparticles with oppositely charged ligands. In these experiments Au and Ag nanoparticles of the same size were modified by ligand exchange with 11-mercaptoundecanoic acid (MUA) and N,N,N-Trimethyl(11-mercaptoundecyl) ammonium chloride (TMA). After titration to achieve a 1:1 ratio, the nanoparticles were redissolved in a mixture of distilled water and a nonpolar non-solvent (DMSO). During heating of this mixed nanoparticle solution at 70 °C over 12 h the water evaporates and the nanoparticles slowly precipitate, so that the dielectric constant (ε) of the mixed solution changes. As is presented in equation [5], when the water, which has a relative dielectric constant of 78, evaporates in the mixture the dielectric constant slowly changes to that of DMSO, which is 65 at 25°C.

Hence, the charge screening is reduced and slow agglomeration starts until the point of complete precipitation is reached.

$$\mathbf{F} = \frac{\mathbf{1}}{\mathbf{4\pi\varepsilon}} \frac{\mathbf{q_1 \cdot q_2}}{\mathbf{r^2}} \quad [5]$$

During their investigations they have also focused on the length scale of the electrostatic interactions. The synthesized mesocrystals crystallize in a diamond like lattice, i.e. every nanoparticle is surrounded by 4 nearest neighbours. This relatively inefficient close packing is as a result of short range interactions; the screening length κ_C^{-1} calculated using Deryagin-Landau-Verwey-Overbeek (DLVO) theory is ~2,7 nm. Additionally, they observed that screening helps the ordered assembly during destabilization because in polydisperse samples smaller particles can stabilize those which are larger so that the long range interactions between them are reduced to the point where flocculation no longer takes place. Too high a polydispersity leads to the complete stabilization of the solution without self-assembly as is shown in Fig. 8.

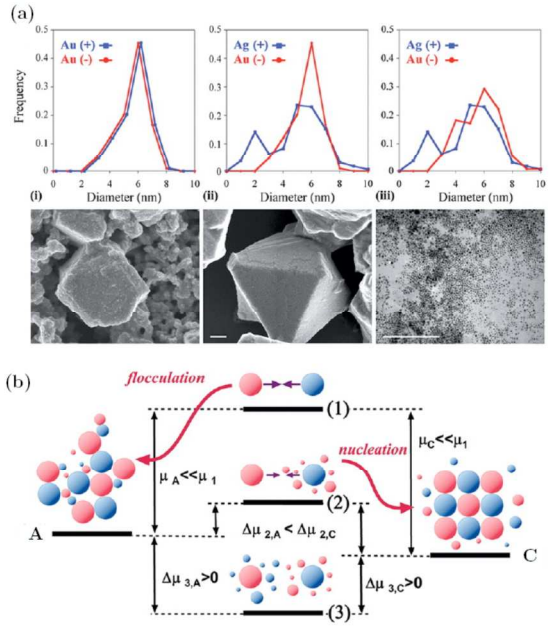

Fig. 8 Electrostatic interactions as driving force for crystallisation. (a) Effect of NP polydispersity on the quality of crystals. Graphs (i) to (iii) give normalised size distributions of the metallic cores of oppositely charged NPs used in crystallisation experiments; typical outcomes of these experiments are illustrated by SEM or TEM images shown in the bottom row (scale bars 200 nm). (b) Effect of small particles on the stability of the dispersed, large NPs. In the absence of small particles (1), large NPs of opposite charges interact by relatively strong electrostatic forces resulting in high chemical potential and the NPs instantly occulate to form amorphous aggregates (A). Small NPs of one type surround large NPs of the opposite charge and effectively screen electrostatic interactions between them (2) so that slow and ordered nucleation takes place. If small NPs of both types are present in the suspension (3), all large NPs are screened and interact very weakly remaining stable solutions. [112]

In addition, external fields such as electrostatic and magnetic fields can also induce self-assembly as polarization forces and permanent dipole moments can orient within such fields. Normally anisotropic nanoparticles arrange along these external fields and form 1D and 2D structures and have even been observed to form 3D structured films.[123–125] The same 1D[126–129], 2D[130,131] and 3D[132,133] structured superlattices are also observed by applying magnetic fields. In addition to the one-dimensional wires chains of rings can also be formed. However, as no symmetrical three-dimensional nanoparticle arrangements have so far been reported to form in such cases we will not focus on this assembly method further.

While the hard sphere model is used to describe the effects of van der Waals, electrostatic, magnetic and dipole interactions within systems composed of nanoparticles, they are better described as core shell systems consisting of a nearly hard inorganic core surrounded by an organic ligand shell. Interactions involving the ligand shell differ from those entailing core-core interactions. Usually, the ligands are organic molecules with different functionalities which can interact with the neighbouring molecules on the same nanoparticle, with molecules on adjacent nanoparticles and/or with solvent molecules. Generally, these interactions are short range, being on the length scale of Angstroms or nanometres, such as covalent bonds, dipole interactions, donor-acceptor interactions and hydrogen bonds to name but a few. These interactions, when separately considered, are weak interactions but their summation over all nanoparticles results in them having a relatively strong effect. As previously described, the solvent influences the magnitude of the interactions, e.g. the dipole-dipole interaction of cis-azobenzene in toluene is $\varepsilon_{dd} \approx 2.7\ kT$ but in water it is $\varepsilon_{dd} \approx 0.08\ kT$, which is as a result of more effective screening due to the higher dielectric constant of water. Hence the molecular dipole interactions of cis-azobenzene in water are too weak to cause significant interaction and therefore charges (not dipoles) are required to induce significant electrostatic interactions.[117] In some cases, these interactions can induce temporary assembly on the mesoscale through changes in environmental conditions or may lead to redissolution of the nanoparticular units. In contrast to the non-directed dipole interactions, donor-acceptor interactions are more specific and hence it is possible to interlink nanoparticles using DNA or other donor-acceptor pairs[134–137], which in future could potentially be more widely used for mesocrystal assembly. Hydrogen bonding is also well documented as being able to provide interactions between ligand molecules and which are stronger in aprotic solvents.[138] In all the above methods the interactions between the ligand molecules play an important role and consequently can influence the mesocrystal morphology. Observations concerning the degree of flexibility of the ligands suggest that stiffness within the ligands may also be important for the formation of ordered and/or non-ordered assemblies induced *via* varying the temperature.[139]

Not only can attractive and repulsive interactions influence mesocrystal formation, but so too can entropic effects. These so called depletion forces and confinement effects (not to be confused with the quantum confinement effects that may be present in the individual building blocks) can be either repulsive or attractive.

The repulsive forces, which are due to the presence of the ligand shell, are primarily due to steric interactions and act to hinder the particles from coming together and therefore prevent their self-assembly.[140,141] These repulsion forces depend on the length and the amount of ligand present at the nanoparticle surface. Attractive entropic interactions result due to the depletion force. Here, hard spheres come together because smaller hard spheres, ligand molecules or solvent molecules are present in the solution, and hence assembly by the bigger nanoparticles is entropically preferred. The force active in keeping the particles together is the osmotic pressure, which acts to push the particles together due to the excluded molecules in between them. This excluded volume or gained volume depends on the size of the depletant.[142,143]

As can be seen the variety of particle interactions that may be present in such systems is large and consequently nearly every interaction leads to new possible mechanistic pathways in the formation of mesocrystals. Also this variety adds a further layer of complexity in trying to understand the formation processes because the self-assembly process always results from an interplay between the different attractive and repulsive forces. Some methods such as that of Grzybowski *et al.* are focused on using electrostatic interactions, others such as those of Talapin and Pileni use van der Waals interactions as well as entropic and ligand interactions. The optimization of the methods employed depends on the combination of nanoparticles, ligand shell, solvent and physical environmental influences such as pressure, temperature and ionic strength of the solvent amongst others. This makes it quite challenging to reproducibly synthesize mesocrystalline materials and a large variation in morphology is present even within the same synthetic batch.

Analogy to Atoms

The analogy of forming a classical crystal from its atomic or molecular components to that of the formation of mesocrystals due to the agglomeration of single nanoparticles into a macroscopic structure is obvious. Despite the fact that the driving forces and the interactions present during the assembly process are somewhat different the resulting structures are nevertheless very similar, as also is the observed growth mechanism. In classical crystallization the first phase in mesocrystal formation is agglomeration caused by supersaturation, with the nanoparticles being destabilized by the addition of non-solvents or the evaporation of solvent. Bodnarchuk *et al.*[101] have observed the in-situ crystal growth process of CdSe, PbS, Au and $CoFe_2O_4$ mesocrystals within a nanoliter microfluidic plug. The nanoparticles are dissolved in an ethanol/toluene droplet and over the time of the toluene evaporation the nanoparticle solution is stable. Only when the nucleation threshold is reached is crystalline material achieved. After this first agglomeration the growth process of these crystals goes on until the solution is completely clear and colourless and as a result mesocrystals were produced that can have different crystalline structures and morphologies. Goubet and Pileni[144] as well as Kalsin *et al.*[112] have demonstrated the analogy between the morphology that results from mesocrystals composed of nanoparticles and that of classical crystals. The mesocrystals show the same crystal facets and angles as the components of classical crystals in the same crystal lattice.

Also twinning effects, which occur in classical crystallization are also found during the self-assembly of mesocrystals. Rupich *et al.*[29] describe the dependence of twinning with respect to the particle size of the constituent PbS nanoparticles and have calculated that with increasing size the twinning becomes more favourable. PbS nanoparticles with a size below 4 nm do not exhibit twinning in the resulting structure. However, by contrast, PbS particles larger than 7 nm in size form multiply twinned face-centred cubic superlattices with decahedral and icosahedral symmetry, exhibiting crystallographically forbidden five-fold symmetry elements. They have also reported that the interparticle potential during agglomeration becomes "softer", which also causes the higher degree of twinning.

Nanoparticle arrangements in colloidal crystals suggest that the principle of maximum space filling is in operation, so that in many experiments an optimized nanoparticle arrangement is observed.[145–150] Experimental data using octahedrally shaped nanoparticles allows the formation of particle arrays, which depend on the composition of the organic ligand shell. [120,145–149,151,152] Four phenomenological models for this observation are proposed:

- anisotropic nanocrystals without or with just a small ligand shell
- hard spheres with small organic shell compared to the core size
- hard spheres with large organic shell compared to the core size
- small hard spheres with a very large organic shell, which is deformable and soft[28]

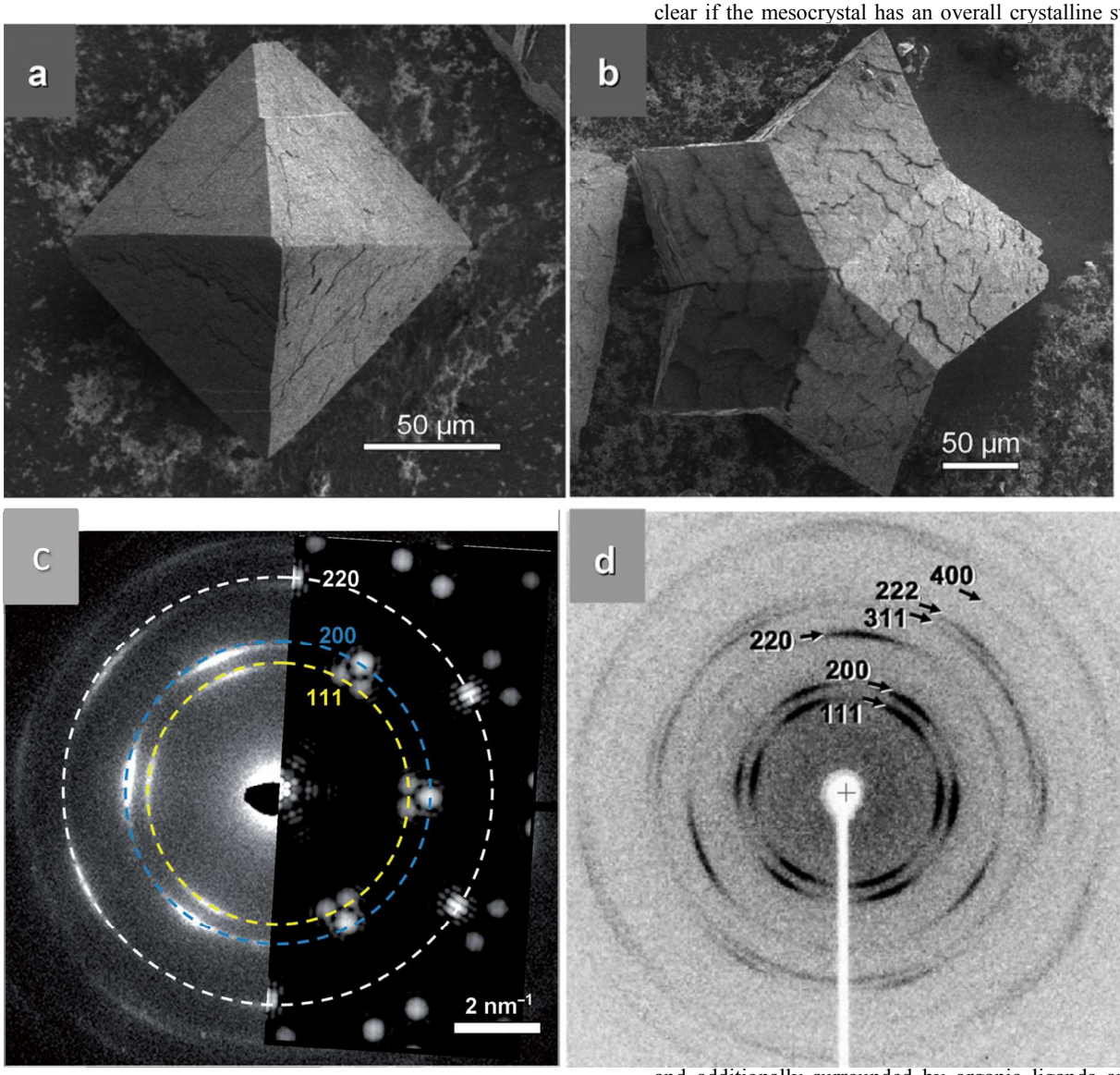

of the observed (left) and simulated (right) ED patterns detected along [111]SL of the PbS–organic mesocrystal. The simulated ED was obtained by superposition of the ED patterns calculated for the proposed models. The sets of equidistant (220), (002), and (111) PbS Bragg reflections are marked with white, blue, and yellow circles, respectively, and d) the corresponding X-ray diffraction pattern (Mo Ka radiation) along [111]SL.[28]

The nanoparticle arrangement between the different models differs and for the nanocrystals without or with a small ligand shell a bcc arrangement is preferred.[149,153] By increasing the coverage of the nanoparticle surface with organic ligand molecules the form of the nanoparticles is smoothened, so that defects in the orientation inside of the super lattice occur. This smoothened surface acts so as to change the packaging from bcc to fcc.[145–147] If small inorganic cores are covered with a thick shell of organics the orientational ordering becomes almost completely lost and the spheres, which can be deformed, arrange in a bcc structure.[148,151] Typically, the crystal structure of mesocrystals can be determined using SAXS measurements however, using this method it is not completely clear if the mesocrystal has an overall crystalline structure or if it

e of a partially
ıe crystal and
M can one
Simon *et al.*[28]
of PbS-organic
the crystalline
seen following
l section of the
ation of the
rom which the
ınt orientation
measurements
ee of mismatch
exists (Fig. 9).
ional ordering
gements in the
ce group could
nanoparticle
face-to-face
ly can possible
meters can be
n calculated to
anocrystals are
anoparticles in

ng applications
e mesocrystals.
t to understand
ials. Zhou and
ation purposes
ed.[154] The first
anic molecules,
nineral bridges
and additionally surrounded by organic ligands and in the third type of mesocrystal the nanoparticles are connected only by mineral bridges but without the presence of organic ligands. These different architectures influence the properties of the single mesocrystal entities, such as the electronic properties and the surface area of the nanoparticles, drastically.

Mesocrystals with bare surfaces show highly accessible surface areas and are well suited for heterogeneous catalysis of gaseous compounds and photocatalysis as shown by Zeng *et al.*[155], Tartaj *et al.*[156] and Yu *et al.*[157]. Zeng *et al.* used CoO and $Zn_{1-x}Co_xO/Co_{1-y}Zn_yO$ nanocomposites to catalyse, in a heterogeneous catalytic reaction, the oxidation of CO to CO_2. Both materials exhibit catalytic activity already at a relatively low temperature of 60°C, which increases up to temperatures of 120-140°C. The high surface area of the synthesised mesocrystalline material and the surface decoration with hydroxyl groups, which are essential for the CO adsorption, are responsible for the high catalytic activity. Yu *et al.* reported on an NO removal *via* a photocatalytic reaction at the surface of TiO_2 nanowires. The mesocrystalline rutile nanowires

show a high catalytic activity because the nanowires have a high aspect ratio, which allows a fast charge transport, a large surface area with many open pores for the diffusion of NO and the efficient penetration of light.

Not only are catalytic reactions on the high surface area of the mesocrystalline materials possible, but in addition these materials are appropriate electrode materials. Pang *et al.* synthesised $W_{18}O_{49}$ mesocrystals, which show good electrochemical properties and have a high electron-proton transport rate. In addition, they show a large pseudocapacitance and a superior stability, which makes them potential materials for use as supercapacitors.

Mesocrystals which possess an organic ligand shell around them and whose preparation was described above, are usually not suitable for use in catalytic approaches as the surfaces are relatively inaccessible but do possess other interesting properties such as closed intracrystalline pores, which is advantageous for thermal and dielectric insulation.

Zhu *et al.* have reported on superstructures and the SERS properties of gold nanocrystals of different shapes.[158] These noble-metal nanocrystal materials possess a plasmon resonance and have many potential applications in e.g. optical waveguides, superlensing, photon detection and surface-enhanced Raman scattering (SERS) for sensing and imaging applications.[158] The SERS sensitivity is highly dependent on the structure of the Au mesocrystals so that the hotspots and the strength of the antenna effect vary. Not only do the size, shape and type of the single building blocks influence the SERS signal, the interparticle distance in the nanoparticle arrangement also changes the signal intensity. The difficulty in this reported study was the production of highly monodisperse Au nanoparticles of different shapes and their controlled assembly into 3D structures. Single-crystalline rhombic dodecahedral nanoparticles arranged into an fcc triangular superstructure showed the highest SERS effect. Additionally, the SERS effect was measured to be stronger along the edges and corners than in the middle of the superstructures. The presence of a higher number of hotspots makes these materials especially interesting as chemical and biological sensors, as immunosensors and for analytical measurements due to their high sensitivity.

The SERS effect was also observed for Ag nanoparticle arrangements as described by Fendler.[159] Additional collective properties of Ag nanoparticles deriving from their shifted resonances in absorption spectroscopy due to Lorentz field effects and changes in reflectance measurements have also been described.[160]

The arrangement of magnetic nanoparticles into ordered superstructures opens up a class of materials with unique magnetic properties. The ferromagnetic nanoparticles so arranged are potential candidates for magnetic storage media. The idea is that each ferromagnetic nanoparticle corresponds to one bit of information. Up to now, there are several challenges to overcome before their application becomes a reality, such as their limited thermal fluctuation and their superparamagnetism at room temperature.[161] Magnetic nanoparticles capped with organic ligands and arranged into mesocrystals show collective behaviour caused by long-range dipolar interactions because contact between the nanoparticles is hindered by the ligand shell so that exchange interactions are neglected.[162] When 3-D ordered and non-ordered arrangements of magnetic nanoparticles are compared, the ordered assemblies possess a more square-like hysteresis loop and a higher blocking temperature, with the consequence that superparamagnet behaviour occurs at higher temperatures. Due to the higher ordering present within mesocrystals, the coupling constant between the nanoparticles increases with decreasing interparticle distance, which corresponds directly to the increase in dipolar interactions.[161] For applications of these magnetic 3D superstructures the interactions between the magnetic nanoparticles and their complicated underlying behaviour need to be investigated further.

The magnetic properties of such mesocrystals can also be used in biomedical and targeting applications. Ge *et al.* have reported on a method by which water soluble Fe_3O_4 mesocrystals that still exhibit superparamagnetism may be produced, which is normally limited in Fe_3O_4 nanoparticles to a domain size of approximately 30 nm.[163,164] Additionally the magnetic response to external magnetic fields, which is caused by the higher magnetization per particle into the arrangement, is much stronger than that of the single magnetic nanoparticles. Coating the mesocrystals with a silica shell allows the coupling via specific silane chemistry ligands to surfaces and molecules.[164]

Another field of application is in the area of photonic crystals. The 3D arrangement of spherical particles into macroscopic ordered structures leads to spatially periodic structures. The nanoparticle sizes need to be in the range of the photon wavelength to influence the propagation of electromagnetic waves. Using template free fabrication of photonic crystals has many advantages e.g. the easily tuneable photonic bandgap *via s*ize variation of the building blocks and relatively inexpensive fabrication. An inherent disadvantages are the imperfect structures that result from 3D self-assembly and, as is often observed, the absence of a full photonic bandgap.

In addition, electronic properties of the isolated nanoparticle arrangements are of great interest. Yang *et al.* investigated the electronic properties of 3D Au colloidal crystals with scanning tunnelling microscope (STM).[165] The STM tip required higher bias voltages because of the insulating organic layers around the nanoparticular building blocks which resulted in a lower effective voltage. Additionally, conductance due to the collective nature of the structure could be observed. In contrast to the conductance of any one given nanocrystal a slight additional modulation was witnessed to be superimposed on the collective conductance background, which mimics the Coulomb staircase structure normally observed from isolated nanoparticles. As most experiments on the electronic behaviour of nanoparticles are made on layers with a defined thickness and size it was also possible to determine that the application of a thermal treatment increases the conductivity[166], which brings these structures one step closer to being used in promising applications involving low-cost, high-performance energy conversion and storage technologies.

Furthermore, Simon et al.[167] have reported on the fibrillation within two dimensional arrangements of PbS nanoparticles, where crystalline PbS bridge-like connections between the individual nanoparticles were observed to form. These crystalline

interconnects could potentially provide the 2D material with good electrical properties and the formation of such interconnects may also extend to the 3D systems that have been reported in the literature[28] using these particles. However, such investigations have yet to show if PbS mesocrystals have potential uses in the field of nanoelectronics and energy conversion.

The mechanical properties of mesocrystals are also of interest with respect to potential applications and therefore it is necessary to understand them with respect to device integration and such parameters as robustness and durability. Measurements have been performed with PbS mesocrystals in the group of Shevchenko *et al.* where the collective mechanical response of the material was undertaken, and which has been reported to be in the range between hard sphere colloidal crystals and opals.[30,168,169] The observed response can be compared with that of hard and stiff polymers, but shows a greater degree of hardness. This increased hardness comes from the dense packing of the spheres, which distributes the stress over the complete material and this results in an increased hardness and modulus. However, the fracture toughness is significantly diminished as only ligand-ligand interactions keep the inorganic cores inside of the material. The ligand-ligand interactions lead to a behaviour which is analogous to stiffness and elasticity in polymers. Podsiadlo *et al.* have also shown the dependence of increasing nanoparticle size on hardness (H) and elasticity (E).[169] If the NP size increases in H then E also increases. The combination of the organic-inorganic core-shell material makes the material behave like nanoparticle-filled polymers. Thus, the mechanical properties can be influenced by ligand-ligand interactions and can be optimized through further investigation. Not only were the mechanical properties of PbS mesocrystals undertaken but also those of Au mesocrystals were measured and it was reported that the formation processes influence the Young's modulus of the different structures.[170] Furthermore, Natalio *et al.*[171] have reported on needle-like calcite crystals with a Young's modulus of 14 GPa. The aligned calcite nanocrystals, with silicatein-α occluded in the domain boundaries, contains between 10 and 16% organic component, which accounts for these remarkable mechanical properties.

Consequently, the relatively high stiffness combined with the elasticity caused by the nanoparticular structure is in accordance with the embedding and integration of these functional materials into technical devices.

All the examples presented here make it clear that the properties of mesocrystals depend on the internal structure of the mesocrystals and hence it is possible to vary and optimize the properties as required for different applications. Both mechanical stability and electrical conductivity are very important characteristics for the integration of the functional materials into devices and first procedures to optimize the materials regarding their conductivity and hardness have been undertaken. It is important for many applications that the mesocrystalline materials are not static materials as is the case for bulk materials. With small changes such as a different ligand shell, the properties can be widely varied and it is possible to optimize the properties with the end application field in mind.

4. Conclusion

In summary, the examples covered within this review illustrate the increasing importance in recent years of non-classical crystallisation mechanisms for providing a fuller description of many complex systems. In particular, their use in elucidating the synthetic pathways involved in oriented attachment and non-classical crystallisation as related to systems in which pre-synthesised nanoparticles are used as building blocks has been focused upon. The advantageous size-tuneable properties of the different nanomaterials can be maintained via their temporal stabilisation in the presence of ligand molecules during mesoscopic assembly. Employing such techniques macroscopic solids, composed of materials whose properties result from various degrees of quantum confinement, and additionally a new set of collective properties that derive from the ordered assembly, can be generated. The analogies between classical crystal lattices and those of nanoparticles are impressive and in some cases the inner structure of the macroscopic solids are so similar to those of classical crystals that, because of the single crystal behaviour of the resulting crystals, the mesocrystal structures can only be identified with thin cut techniques such as focused ion beam techniques. Additionally this review provides an overview of the techniques that can be employed to provide structuring as well as the possible interparticle interactions that influence the resulting arrangements to provide further property variations and applications. While much has been achieved in order to attain our present state of understanding, there is certainly much additional fundamental work yet to be done in order to more fully characterise the interactions at work in such systems, and in particular the length scales over which they effectively operate. However, such investigations will be necessary if we are to comprehend with greater clarity how to ultimately control the structuring and properties of mesocrystalline solids and even more so if we are to utilise them in such a way as to reach their full application potential.

Acknowledgements

This work was supported by the DFG Research Training Group 'Nano- and Biotechniques for the Packaging of Electronic Systems' (DFG 1401/2).

Notes and references

Physical Chemistry, TU Dresden Bergstraße 66b, 01062 Dresden, Germany Fax: +49 351 463-37164; Tel: +49 351 463-37597; E-mail: S.Hickey@chemie.tu-dresden.de

1. E. H. Falcao and F. Wudl, *J. Chem. Technol. Biotechnol.*, 2007, **82**, 524–531.

2. J. A. Dirksen and T. A. Ring, *Chem. Eng. Sci.*, 1991, **46**, 2389–2427.

3. R. A. Van Santen, *J. Phys. Chem.*, 1984, **88**, 5768–5769.

4. C. B. Murray, C. R. Kagan, and M. G. Bawendi, *Annu. Rev. Mater. Sci.*, 2000, **30**, 545–610.

5. X. Peng, J. Wickham, and A. P. Alivisatos, *J. Am. Chem. Soc.*, 1998, **120**, 5343–5344.

6. G. H. Nancollas, Ed., *Biological Mineralization and Demineralization*, Springer Berlin Heidelberg, Berlin, Heidelberg, 1982.

7. C. J. Dalmaschio, C. Ribeiro, and E. R. Leite, *Nanoscale*, 2010, **2**, 2336–45.

8. V. K. LaMer and R. H. Dinegar, *J. Am. Chem. Soc.*, 1950, **72**, 4847–4854.

9. H. Goesmann and C. Feldmann, *Angew. Chem. Int. Ed. Engl.*, 2010, **49**, 1362–95.

10. G. Wulff, *Zeitschrift für Krist.*, 1901, **34**, 449–480.

11. J.-H. Zhang, Y. Zhang, Y.-H. Wen, and Z.-Z. Zhu, *Comput. Mater. Sci.*, 2010, **48**, 250–257.

12. W. Kossel, *Ann. Phys.*, 1934, **413**, 457–480.

13. H. Cölfen and M. Antonietti, *Mesocrystals and Nonclassical Crystallization*, Wiley New York, 2008.

14. Y. Ma, H. Cölfen, and M. Antonietti, *J. Phys. Chem. B*, 2006, **110**, 10822–8.

15. S.-H. Yu and H. Cölfen, *J. Mater. Chem.*, 2004, **14**, 2124.

16. H. Tlatlik, P. Simon, A. Kawska, D. Zahn, and R. Kniep, *Angew. Chem. Int. Ed. Engl.*, 2006, **45**, 1905–10.

17. N. Gehrke, N. Nassif, N. Pinna, M. Antonietti, H. S. Gupta, and H. Cölfen, *Chem. Mater.*, 2005, **17**, 6514–6516.

18. M. Balz, H. A. Therese, J. Li, J. S. Gutmann, M. Kappl, L. Nasdala, W. Hofmeister, H.-J. Butt, and W. Tremel, *Adv. Funct. Mater.*, 2005, **15**, 683–688.

19. L. Qi, H. Cölfen, and M. Antonietti, *Chem. Eur. J.*, 2001, 3526–3532.

20. M. Faatz, F. Gröhn, and G. Wegner, *Adv. Mater.*, 2004, **16**, 996–1000.

21. M. Faatz, F. Gröhn, and G. Wegner, *Mater. Sci. Eng. C*, 2005, **25**, 153–159.

22. E. DiMasi, S.-Y. Kwak, F. Amos, M. Olszta, D. Lush, and L. Gower, *Phys. Rev. Lett.*, 2006, **97**, 045503.

23. L. . Gower and D. . Tirrell, *J. Cryst. Growth*, 1998, **191**, 153–160.

24. L. Addadi and S. Weiner, *Angew. Chemie Int. Ed. English*, 1992, **31**, 153–169.

25. L. B. Gower, *Chem. Rev.*, 2008, **108**, 4551–627.

26. G. Cao, *Nanostructures and Nanopmaterials - Synthesis, Properties and Applications*, Imperial College Press, London, 2004.

27. M. Niederberger and H. Cölfen, *Phys. Chem. Chem. Phys.*, 2006, **8**, 3271–87.

28. P. Simon, E. Rosseeva, I. A. Baburin, L. Liebscher, S. G. Hickey, R. Cardoso-Gil, A. Eychmüller, R. Kniep, and W. Carrillo-Cabrera, *Angew. Chem. Int. Ed. Engl.*, 2012, **51**, 10776–81.

29. S. M. Rupich, E. V. Shevchenko, M. I. Bodnarchuk, B. Lee, and D. V. Talapin, *J. Am. Chem. Soc.*, 2010, **132**, 289–96.

30. P. Podsiadlo, G. Krylova, B. Lee, K. Critchley, D. J. Gosztola, D. V. Talapin, P. D. Ashby, and E. V. Shevchenko, *J. Am. Chem. Soc.*, 2010, **132**, 8953–60.

31. T. Vossmeyer, G. Reck, L. Katsikas, E. T. Haupt, B. Schulz, and H. Weller, *Science*, 1995, **267**, 1476–9.

32. C. B. Murray, S. Sun, W. Gaschler, H. Doyle, T. A. Betley, and C. R. Kagan, *IBM J. Res. Dev.*, 2001, **45**, 47–56.

33. D. V. Talapin, E. V. Shevchenko, A. Kornowski, N. Gaponik, M. Haase, A. L. Rogach, and H. Weller, *Adv. Mater.*, 2001, **13**, 1868.

34. J. Fang, X. Ma, H. Cai, X. Song, and B. Ding, *Nanotechnology*, 2006, **17**, 5841–5845.

35. J. Fang, B. Ding, and X. Song, *Appl. Phys. Lett.*, 2007, **91**, 083108.

36. S.-H. Yu, H. Cölfen, K. Tauer, and M. Antonietti, *Nat. Mater.*, 2005, **4**, 51–5.

37. X.-H. Guo and S.-H. Yu, *Cryst. Growth Des.*, 2007, **7**, 354–359.

38. A.-W. Xu, M. Antonietti, H. Cölfen, and Y.-P. Fang, *Adv. Funct. Mater.*, 2006, **16**, 903–908.

39. M. G. Page and H. Cölfen, *Cryst. Growth Des.*, 2006, **6**, 1915–1920.

40. T. Wang, M. Antonietti, and H. Cölfen, *Chem. - A Eur. J.*, 2006, **12**, 5722–30.

41. J. Zhan, H.-P. Lin, and C.-Y. Mou, *Adv. Mater.*, 2003, **15**, 621–623.

42. Olaf Grassman, R. B. Neder, A. P. And, and P. Löbmann, *Am. Mineral.*, 2003, **88**, 647–652.

43. O. Grassmann and P. Löbmann, *Biomaterials*, 2004, **25**, 277–282.

44. O. Grassmann, G. Müller, and P. Löbmann, *Chem. Mater.*, 2002, **14**, 4530–4535.

45. T. Wang, H. Cölfen, and M. Antonietti, *J. Am. Chem. Soc.*, 2005, **127**, 3246–7.

46. O. Grassmann and P. Löbmann, *Chemistry*, 2003, **9**, 1310–6.

47. O. Pujol, P. Bowen, P. A. Stadelmann, and H. Hofmann, *J. Phys. Chem. B*, 2004, **108**, 13128–13136.

48. E. V. Shevchenko, D. V. Talapin, A. L. Rogach, A. Kornowski, M. Haase, and H. Weller, *J. Am. Chem. Soc.*, 2002, **124**, 11480–11485.

49. S. Wohlrab, N. Pinna, M. Antonietti, and H. Cölfen, *Chemistry*, 2005, **11**, 2903–13.

50. Y. Oaki, A. Kotachi, T. Miura, and H. Imai, *Adv. Funct. Mater.*, 2006, **16**, 1633–1639.

51. J. Seto, Y. Ma, S. A. Davis, F. Meldrum, A. Gourrier, Y.-Y. Kim, U. Schilde, M. Sztucki, M. Burghammer, S. Maltsev, C. Jäger, and H. Cölfen, *Proc. Natl. Acad. Sci. U. S. A.*, 2012, **109**, 3699–704.

52. L. Zhou and P. O'Brien, *J. Phys. Chem. Lett.*, 2012, **3**, 620–628.

53. J. F. Banfield, *Science (80-.).*, 2000, **289**, 751–754.

54. R. L. Penn, *Science (80-.).*, 1998, **281**, 969–971.

55. R. L. Penn and J. F. Banfield, *Geochim. Cosmochim. Acta*, 1999, **63**, 1549–1557.

56. E. J. H. Lee, C. Ribeiro, E. Longo, and E. R. Leite, *J. Phys. Chem. B*, 2005, **109**, 20842–6.

57. E. R. Leite, T. R. Giraldi, F. M. Pontes, E. Longo, A. Beltrán, and J. Andrés, *Appl. Phys. Lett.*, 2003, **83**, 1566.

58. J. Polleux, N. Pinna, M. Antonietti, C. Hess, U. Wild, R. Schlögl, and M. Niederberger, *Chem. - A Eur. J.*, 2005, **11**, 3541–51.

59. C. Ribeiro, E. J. H. Lee, E. Longo, and E. R. Leite, *Chemphyschem*, 2005, **6**, 690–6.

60. R. L. Penn, *J. Phys. Chem. B*, 2004, **108**, 12707–12712.

61. J. Zhang, F. Huang, and Z. Lin, *Nanoscale*, 2010, **2**, 18–34.

62. H. G. Yang and H. C. Zeng, *Angew. Chemie*, 2004, **116**, 6056–6059.

63. H. C. Zeng, *J. Mater. Chem.*, 2006, **16**, 649.

64. J. Zhang, Z. Lin, Y. Lan, G. Ren, D. Chen, F. Huang, and M. Hong, *J. Am. Chem. Soc.*, 2006, **128**, 12981–7.

65. K.-S. Cho, D. V. Talapin, W. Gaschler, and C. B. Murray, *J. Am. Chem. Soc.*, 2005, **127**, 7140–7.

66. V. M. Yuwono, N. D. Burrows, J. A. Soltis, and R. L. Penn, *J. Am. Chem. Soc.*, 2010, **132**, 2163–5.

67. John A. Venables, *Introduction to Surface and Thin Film Processes*, Cambridge University Press, 2000.

68. S. Kudera, L. Carbone, M. F. Casula, R. Cingolani, A. Falqui, E. Snoeck, W. J. Parak, and L. Manna, *Nano Lett.*, 2005, **5**, 445–9.

69. A. A. Chernov, *J. Cryst. Growth*, 1974, **24-25**, 11–31.

70. Z. Tang, N. A. Kotov, and M. Giersig, *Science*, 2002, **297**, 237–40.

71. C. Pacholski, A. Kornowski, and H. Weller, *Angew. Chem. Int. Ed. Engl.*, 2002, **41**, 1188–91.

72. A. Halder and N. Ravishankar, *Adv. Mater.*, 2007, **19**, 1854–1858.

73. H. Cölfen and M. Antonietti, *Angew. Chemie (International ed.)*, 2005, **44**, 5576–91.

74. C. M. Soukoulis, *Phys. Scr.*, 1996, **T66**, 146–150.

75. C. Murray, C. Kagan, and M. Bawendi, *Science (80-.).*, 1995, **270**, 1335–1338.

76. W. Hsu, L. Ronnquist, and E. Matijevic, *Langmuir*, 1988, **17**, 31–37.

77. J. J. Petres, G. Deželić, and B. Težak, *Croat. Chem. Acta*, 1969, **41**, 183–186.

78. S.-H. Lee, Y.-S. Her, and E. Matijević, *J. Colloid Interface Sci.*, 1997, **186**, 193–202.

79. Z. Zhang, H. Sun, X. Shao, D. Li, H. Yu, and M. Han, *Adv. Mater.*, 2005, **17**, 42–47.

80. M. Ball and H. Taylor, *Mineral. Mag.*, 1961, 754–766.

81. N. Thangaraj, K. H. Westmacott, and U. Dahmen, *Ultramicroscopy*, 1991, **37**, 362–374.

82. J. Bernal, D. Dasgupta, and A. Mackay, *Nature*, 1957.

83. H. Bärnighausen, *Zeitschrift für Anorg. und Allg. Chemie*, 1967, **349**, 280–288.

84. H. Bärnighausen, *Zeitschrift für Anorg. und Allg. Chemie*, 1970, **374**, 201–224.

85. S. Dominguez Bella and J. M. Garcia-Ruiz, *J. Cryst. Growth*, 1986, **79**, 236–240.

86. C. P. Collier, T. Vossmeyer, and J. R. Heath, *Annu. Rev. Phys. Chem.*, 1998, **49**, 371–404.

87. C. Schliehe, B. H. Juarez, M. Pelletier, S. Jander, D. Greshnykh, M. Nagel, A. Meyer, S. Foerster, A. Kornowski, C. Klinke, and H. Weller, *Science*, 2010, **329**, 550–3.

88. Z. Wang, C. Schliehe, K. Bian, D. Dale, W. a Bassett, T. Hanrath, C. Klinke, and H. Weller, *Nano Lett.*, 2013, **13**, 1303–11.

89. D. V. Talapin, E. V. Shevchenko, M. I. Bodnarchuk, X. Ye, J. Chen, and C. B. Murray, *Nature*, 2009, **461**, 964–7.

90. J. J. Urban, D. V. Talapin, E. V. Shevchenko, and C. B. Murray, *J. Am. Chem. Soc.*, 2006, **128**, 3248–55.

91. S. I. Stoeva, B. L. V. Prasad, S. Uma, P. K. Stoimenov, V. Zaikovski, C. M. Sorensen, and K. J. Klabunde, *J. Phys. Chem. B*, 2003, **107**, 7441–7448.

92. R. P. Andres, J. D. Bielefeld, J. I. Henderson, D. B. Janes, V. R. Kolagunta, C. P. Kubiak, W. J. Mahoney, and R. G. Osifchin, *Science (80-.).*, 1996, **273**, 1690–1693.

93. R. Kniep and S. Busch, *Angew. Chemie Int. Ed. English*, 1996, **35**, 2624–2626.

94. S. Busch, H. Dolhaine, A. DuChesne, S. Heinz, O. Hochrein, F. Laeri, O. Podebrad, U. Vietze, T. Weiland, and R. Kniep, *Eur. J. Inorg. Chem.*, 1999, **1999**, 1643–1653.

95. S. Busch, U. Schwarz, and R. Kniep, *Chem. Mater.*, 2001, **13**, 3260–3271.

96. S. Busch, U. Schwarz, and R. Kniep, *Adv. Funct. Mater.*, 2003, **13**, 189–198.

97. P. Simon, U. Schwarz, and R. Kniep, *J. Mater. Chem.*, 2005, **15**, 4992.

98. R. Kniep and P. Simon, *Biominer. I*, 2007, 73–125.

99. A. Putnis, M. Prieto, and L. Fernandez-Diaz, *Geol. Mag.*, 2009, **132**, 1.

100. M. Nagel, S. G. Hickey, A. Frömsdorf, A. Kornowski, and H. Weller, *Zeitschrift für Phys. Chemie*, 2007, **221**, 427–437.

101. M. I. Bodnarchuk, L. Li, A. Fok, S. Nachtergaele, R. F. Ismagilov, and D. V. Talapin, *J. Am. Chem. Soc.*, 2011, **133**, 8956–60.

102. N. Zheng, J. Fan, and G. D. Stucky, *J. Am. Chem. Soc.*, 2006, **128**, 6550–1.

103. A. Courty, *J. Phys. Chem. C*, 2010, **114**, 3719–3731.

104. M. I. Bodnarchuk, M. V Kovalenko, W. Heiss, and D. V. Talapin, *J. Am. Chem. Soc.*, 2010, **132**, 11967–77.

105. W. H. Evers, B. De Nijs, L. Filion, S. Castillo, M. Dijkstra, and D. Vanmaekelbergh, *Nano Lett.*, 2010, **10**, 4235–41.

106. K. Overgaag, W. Evers, B. de Nijs, R. Koole, J. Meeldijk, and D. Vanmaekelbergh, *J. Am. Chem. Soc.*, 2008, **130**, 7833–5.

107. D. V. Talapin, E. V. Shevchenko, C. B. Murray, A. V Titov, and P. Kral, *Nano Lett.*, 2007, **7**, 1213–9.

108. M. Agthe, E. Wetterskog, J. Mouzon, G. Salazar-Alvarez, and L. Bergström, *CrystEngComm*, 2014, **16**, 1443.

109. C.-W. Liao, Y.-S. Lin, K. Chanda, Y.-F. Song, and M. H. Huang, *J. Am. Chem. Soc.*, 2013, **135**, 2684–93.

110. N. Goubet, J. Richardi, P. A. Albouy, and M. P. Pileni, *J. Phys. Chem. Lett.*, 2011, **2**, 417–422.

111. N. Goubet, H. Portalès, C. Yan, I. Arfaoui, P.-A. Albouy, A. Mermet, and M. P. Pileni, *J. Am. Chem. Soc.*, 2012, **134**, 3714–9.

112. A. M. Kalsin, M. Fialkowski, M. Paszewski, S. K. Smoukov, K. J. M. Bishop, and B. A. Grzybowski, *Science*, 2006, **312**, 420–4.

113. B. Kowalczyk, A. M. Kalsin, R. Orlik, K. J. M. Bishop, A. Z. Patashinskii, A. Mitus, and B. a Grzybowski, *Chemistry*, 2009, **15**, 2032–5.

114. B. Kowalczyk, D. A. Walker, S. Soh, and B. A. Grzybowski, *Angew. Chem. Int. Ed. Engl.*, 2010, **49**, 5737–41.

115. K. J. M. Bishop and B. Grzybowski, *Chemphyschem*, 2007, **8**, 2171–6.

116. R. Orlik, A. C. Mitus, B. Kowalczyk, A. Z. Patashinski, and B. A. Grzybowski, *J. Non. Cryst. Solids*, 2009, **355**, 1360–1369.

117. K. J. M. Bishop, C. E. Wilmer, S. Soh, and B. A. Grzybowski, *Small*, 2009, **5**, 1600–30.

118. T. Miura, A. Kotachi, Y. Oaki, and H. Imai, *Cryst. Growth Des.*, 2006, **6**, 612–615.

119. Y. Oaki and H. Imai, *Small*, 2006, **2**, 66–70.

120. S. A. Harfenist, Z. L. Wang, M. M. Alvarez, I. Vezmar, and R. L. Whetten, *J. Phys. Chem.*, 1996, **100**, 13904–13910.

121. L. Hill Terrell, *Statistical mechanics / principles and selected applications*, New York : McGraw-Hill, 1956.

122. N. Goubet, J. Richardi, P.-A. Albouy, and M. P. Pileni, *Adv. Funct. Mater.*, 2011, **21**, 2693–2704.

123. K. M. Ryan, A. Mastroianni, K. A. Stancil, H. Liu, and A. P. Alivisatos, *Nano Lett.*, 2006, **6**, 1479–82.

124. P. A. Smith, C. D. Nordquist, T. N. Jackson, T. S. Mayer, B. R. Martin, J. Mbindyo, and T. E. Mallouk, *Appl. Phys. Lett.*, 2000, **77**, 1399.

125. B. M. I. van der Zande, G. J. M. Koper, and H. N. W. Lekkerkerker, *J. Phys. Chem. B*, 1999, **103**, 5754–5760.

126. M. Tanase, D. M. Silevitch, A. Hultgren, L. A. Bauer, P. C. Searson, G. J. Meyer, and D. H. Reich, *J. Appl. Phys.*, 2002, **91**, 8549.

127. M. Tanase, E. J. Felton, D. S. Gray, A. Hultgren, C. S. Chen, and D. H. Reich, *Lab Chip*, 2005, **5**, 598–605.

128. S. L. Tripp, S. V. Pusztay, A. E. Ribbe, and A. Wei, *J. Am. Chem. Soc.*, 2002, **124**, 7914–7915.

129. S. L. Tripp, R. E. Dunin-Borkowski, and A. Wei, *Angew. Chem. Int. Ed. Engl.*, 2003, **42**, 5591–3.

130. U. Wiedwald, M. Spasova, M. Farle, M. Hilgendorff, and M. Giersig, *J. Vac. Sci. Technol. A Vacuum, Surfaces, Film.*, 2001, **19**, 1773.

131. Y. Lalatonne, J. Richardi, and M. P. Pileni, *Nat. Mater.*, 2004, **3**, 121–5.

132. M. P. Pileni, *J. Phys. Chem. B*, 2001, **105**, 3358–3371.

133. S. Sun and C. B. Murray, *J. Appl. Phys.*, 1999, **85**, 4325.

134. A. P. Alivisatos, K. P. Johnsson, X. Peng, T. E. Wilson, C. J. Loweth, M. P. Bruchez, and P. G. Schultz, *Nature*, 1996, **382**, 609–11.

135. H. Yan, S. H. Park, G. Finkelstein, J. H. Reif, and T. H. LaBean, *Science*, 2003, **301**, 1882–4.

136. E. Braun, Y. Eichen, U. Sivan, and G. Ben-Yoseph, *Nature*, 1998, **391**, 775–8.

137. C. A. Mirkin, R. L. Letsinger, R. C. Mucic, and J. J. Storhoff, *Nature*, 1996, **382**, 607–9.

138. T. Steiner, *Angew. Chemie Int. Ed.*, 2002.

139. P. Born, E. Murray, and T. Kraus, *J. Phys. Chem. Solids*, 2010, **71**, 95–99.

140. E. P. K. Currie, W. Norde, and M. A. Cohen Stuart, *Adv. Colloid Interface Sci.*, 2003, **100-102**, 205–265.

141. S. Milner, *Science (80-.).*, 1991, **251**, 905–914.

142. F. Oosawa, *J. Chem. Phys.*, 1954, **22**, 1255.

143. D. Baranov, A. Fiore, M. van Huis, C. Giannini, A. Falqui, U. Lafont, H. Zandbergen, M. Zanella, R. Cingolani, and L. Manna, *Nano Lett.*, 2010, **10**, 743–9.

144. N. Goubet and M. P. Pileni, *J. Phys. Chem. Lett.*, 2011, **2**, 1024–1031.

145. Z. Quan and J. Fang, *Nano Today*, 2010, **5**, 390–411.

146. J. J. Choi, C. R. Bealing, K. Bian, K. J. Hughes, W. Zhang, D.-M. Smilgies, R. G. Hennig, J. R. Engstrom, and T. Hanrath, *J. Am. Chem. Soc.*, 2011, **133**, 3131–8.

147. K. Bian, J. J. Choi, A. Kaushik, P. Clancy, D. Smilgies, and T. Hanrath, *ACS Nano*, 2011, **5**, 2815–23.

148. B. W. Goodfellow and B. a Korgel, *ACS Nano*, 2011, **5**, 2419–24.

149. R. K. Zheng, H. Gu, B. Xu, K. K. Fung, X. X. Zhang, and S. P. Ringer, *Adv. Mater.*, 2006, **18**, 2418–2421.

150. S. C. Glotzer and M. J. Solomon, *Nat. Mater.*, 2007, **6**, 557–62.

151. B. a. Korgel, S. Fullam, S. Connolly, and D. Fitzmaurice, *J. Phys. Chem. B*, 1998, **102**, 8379–8388.

152. R. L. Whetten, M. N. Shafigullin, J. T. Khoury, T. G. Schaaff, I. Vezmar, M. M. Alvarez, and A. Wilkinson, *Acc. Chem. Res.*, 1999, **32**, 397–406.

153. U. Agarwal and F. a Escobedo, *Nat. Mater.*, 2011, **10**, 230–5.

154. L. Zhou and P. O'Brien, *Small*, 2008, **4**, 1566–74.

155. K. X. Yao and H. C. Zeng, *J. Phys. Chem. C*, 2009, **113**, 1373–1385.

156. P. Tartaj, *Chem. Commun. (Camb).*, 2011, **47**, 256–8.

157. D. Zhang, G. Li, F. Wang, and J. C. Yu, *CrystEngComm*, 2010, **12**, 1759.

158. Z. Zhu, H. Meng, W. Liu, X. Liu, J. Gong, X. Qiu, L. Jiang, D. Wang, and Z. Tang, *Angew. Chem. Int. Ed. Engl.*, 2011, **50**, 1593–6.

159. J. H. Fendler, in *Nanocrystals Forming Mesoscopic Structures*, Wiley-VCH Verlag GmbH & Co. KGaA, Weinheim, 2005, pp. 279–293.

160. A. Brioude, A. Courty, and M. P. Pileni, in *Nanocrystals Forming Mesoscopic Structures*, Wiley-VCH Verlag GmbH & Co. KGaA, Weinheim, 2005, pp. 213–229.

161. C. Petit, L. Motte, A. Ngo, I. Lisiecki, and M. P. Pileni, in *Nanocrystals Forming Mesoscopic Structures*, Wiley-VCH Verlag GmbH & Co. KGaA, Weinheim, 2005, pp. 251–278.

162. R. Chantrell, N. Walmsley, J. Gore, and M. Maylin, *Phys. Rev. B*, 2000, **63**, 024410.

163. R.-Q. Song and H. Cölfen, *Adv. Mater.*, 2010, **22**, 1301–30.

164. J. Ge, Y. Hu, M. Biasini, W. P. Beyermann, and Y. Yin, *Angew. Chem. Int. Ed. Engl.*, 2007, **46**, 4342–5.

165. P. Yang, I. Arfaoui, T. Cren, N. Goubet, and M. P. Pileni, *Nano Lett.*, 2012, **12**, 2051–5.

166. T. Hanrath, *J. Vac. Sci. Technol. A Vacuum, Surfaces, Film.*, 2012, **30**, 030802.

167. P. Simon, L. Bahrig, I. A. Baburin, P. Formanek, F. Röder, J. Sickmann, S. G. Hickey, A. Eychmüller, H. Lichte, R. Kniep, and E. Rosseeva, *Adv. Mater.*, 2014.

168. E. Tam, P. Podsiadlo, E. Shevchenko, D. F. Ogletree, M.-P. Delplancke-Ogletree, and P. D. Ashby, *Nano Lett.*, 2010, **10**, 2363–7.

169. P. Podsiadlo, B. Lee, V. B. Prakapenka, G. V Krylova, R. D. Schaller, A. Demortière, and E. V. Shevchenko, *Nano Lett.*, 2011, **11**, 579–88.

170. C. Yan, I. Arfaoui, N. Goubet, and M. P. Pileni, *Adv. Funct. Mater.*, 2013, **23**, 2315–2321.

171. F. Natalio, T. P. Corrales, M. Panthöfer, D. Schollmeyer, I. Lieberwirth, W. E. G. Müller, M. Kappl, H.-J. Butt, and W. Tremel, *Science*, 2013, **339**, 1298–302.

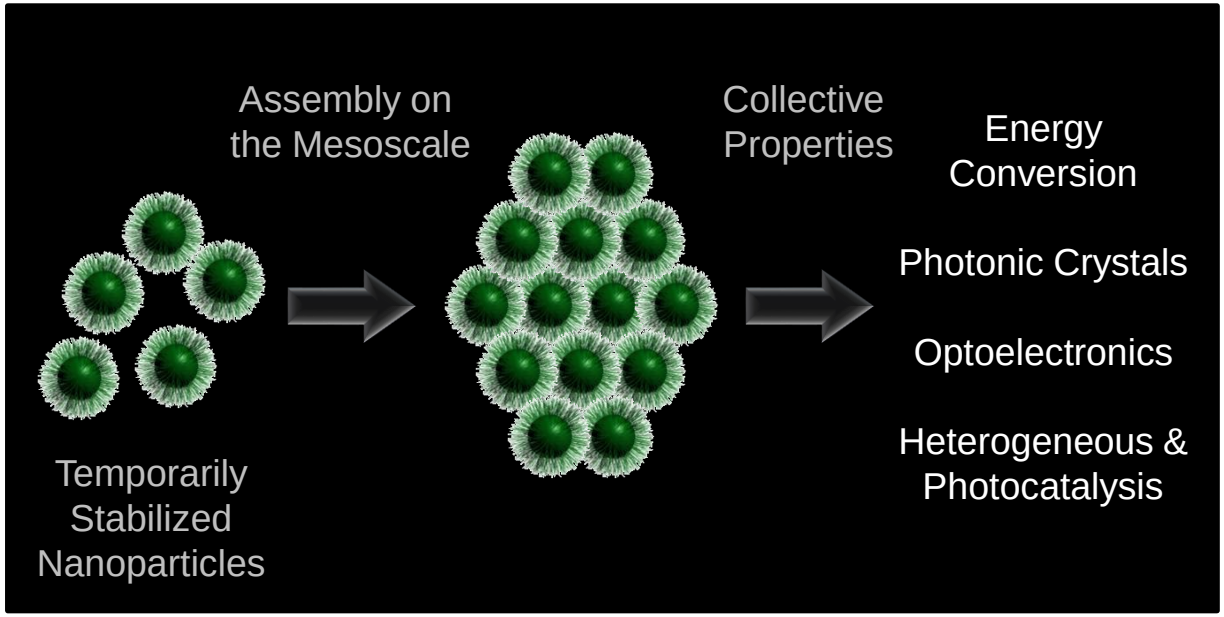

"In this work the oriented attachment and mesocrystal formation via non-classical pathways have been reviewed with particular emphasis being placed on their self-assembly mechanisms as well as the new collective properties of the resulting crystalline nanoparticular arrangements and their potential uses in applications."